Environmental Science & Technology

pubs.acs.org/est

Article

Mercury Accumulation and Sequestration in a Deglaciated Forest Chronosequence: Insights from Particulate and Mineral-Associated Forms of Organic Matter

Fei Wu, Luhan Yang, Xun Wang,* Wei Yuan, Che-Jen Lin, and Xinbin Feng

Cite This: *Environ. Sci. Technol.* 2023, 57, 16512−16521

Read Online

ACCESS | Metrics & More | Article Recommendations | Supporting Information

ABSTRACT: Understanding mercury (Hg) complexation with soil organic matter is important in assessing atmospheric Hg accumulation and sequestration processes in forest ecosystems. Separating soil organic matter into particulate organic matter (POM) and mineral-associated organic matter (MAOM) can help in the understanding of Hg dynamics and cycling due to their very different chemical constituents and associated formation and functioning mechanisms. The concentration of Hg, carbon, and nitrogen contents and isotopic signatures of POM and MAOM in a deglaciated forest chronosequence were determined to construct the processes of Hg accumulation and sequestration. The results show that Hg in POM and MAOM are mainly derived from atmospheric Hg^0 deposition. Hg concentration in MAOM is up to 76% higher than that in POM of broadleaf forests and up to 60% higher than that in POM of coniferous forests. Hg accumulation and sequestration in organic soil vary with the vegetation succession. Variations of $\delta^{202}Hg$ and $\Delta^{199}Hg$ are controlled by source mixing in the broadleaf forest and by Hg sequestration processes in the coniferous forest. Accumulation of atmospheric Hg and subsequent microbial reduction enrich heavier Hg isotopes in MAOM compared to POM due to the specific chemical constituents and nutritional role of MAOM.

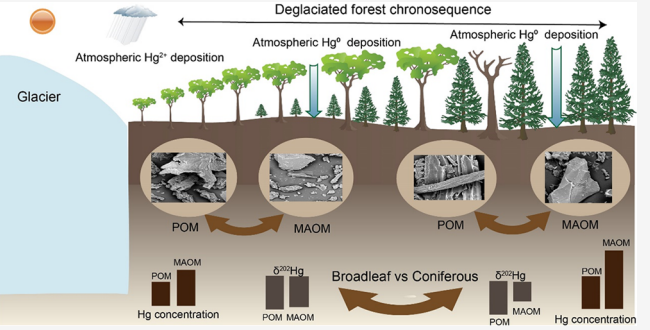

KEYWORDS: *mercury, isotopes, mineral-associated organic matter, particulate organic matter*

1. INTRODUCTION

Mercury (Hg) is a persistent pollutant that causes health and ecological concerns across the globe.[1−3] Forests play an important role in global Hg cycling. It acts as an atmospheric Hg sink with a deposition flux of 2200−3400 Mg yr^{-1},[4,5] and represents the largest terrestrial Hg pool with 500−1100 Gg of Hg stored in surface soil and vegetation.[5,6] Hg cycling in forest ecosystems is closely associated with carbon (C) cycling. Complex formation between soil Hg and organic matter largely controls atmospheric Hg accumulation and sequestration in forests.[5−8] Earlier studies have attempted to explain the complexation mechanisms through analysis of stoichiometry among Hg, C, and nitrogen (N),[9−11] kinetic measurements,[12−14] and speciation of molecular components.[15,16] It is found that soil organic matter plays a complicated, yet not well-understood, role in Hg cycling after deposition on forest soil.

Soil organic matter is a complex mixture that can be separated into multiple components of diverse properties.[17,18] Analyzing the difference of soil organic matter in particulate (POM) and mineral-associated (MAOM) has demonstrated potential in process understanding since the two organic components form, behave, and function distinctly.[17−21] POM is largely made up of lightweight fragments decomposed from litters and has a residence time of <10 years in soils.[17−21] MAOM consists of single molecules and microscopic fragments of organic material formed from leached fraction of decomposing litters, including compounds transformed by soil biota with decades to centuries residence time.[18,20] The differentiation of POM from MAOM enables a more accurate prediction of persistence, dynamics, and cycling in organic soil[17−21] and therefore provides further understanding of Hg complexed with soil organic matter. Compared to POM, MAOM is nutrient-rich, has a lower C/N ratio, and contains fewer plant-derived compounds and more microbial products.[17−21] Previous studies suggested enhanced Hg accumulation in "old soil organic matter" and speculated that Hg is preferentially sorbed to high-density metal-binding functional groups.[7,11,22,23] This indicates that MAOM has a higher adsorption ability of Hg compared to POM.

Received: April 24, 2023
Revised: October 4, 2023
Accepted: October 5, 2023
Published: October 19, 2023

https://doi.org/10.1021/acs.est.3c03107
Environ. Sci. Technol. 2023, 57, 16512−16521

The Hg-stable isotope values can be utilized for tracing Hg accumulation and sequestration in POM and MAOM. The three unique dimensions of Hg isotopic fractionation, i.e., the mass dependent fractionation (MDF, mainly represented by δ^{202}Hg), odd mass independent fractionation (odd-MIF, reported as Δ^{199}Hg and Δ^{201}Hg), and even mass independent fractionation (even-MIF, reported as Δ^{200}Hg and Δ^{204}Hg) are particularly useful. Earlier studies have documented the mechanisms and isotopic fractionations of Hg biogeochemical processes in soil.[5,6,24,25] The microbial reductions in soil only induce Hg MDF.[26,27] Dark oxidation or reduction of soil organic matter is usually associated with small negative odd-MIF in reactants.[25,28] Photoreduction on the interface between air and soil leads to a relatively large positive odd-MIF in the product Hg^0 of S-containing organic ligands.[24,29] Hg contributed from different sources exhibits distinct isotopic signatures. Three source endmembers have been identified for soil Hg in forests, including atmospheric Hg^{2+} deposition, atmospheric Hg^0 deposition, and geogenic sources (i.e., Hg releasing from process of rock weathering). Hg^{2+} in precipitation shows negative δ^{202}Hg, positive Δ^{199}Hg, and Δ^{200}Hg signals.[30−33] Atmospheric Hg^0 in remote regions shows slightly negative Δ^{199}Hg signatures, negative Δ^{200}Hg signatures,[28,34−36] and small δ^{202}Hg signatures.[5,37] Geogenic Hg sources generally feature negative δ^{202}Hg, negligible Δ^{199}Hg, and Δ^{200}Hg signals.[2,38] Therefore, the dynamics of Hg isotopic signatures in POM and MAOM would reflect variations in Hg biogeochemical processes due to their distinct chemical constituents and nutritional roles. Thus, information on Hg content variations and isotopic shifts between POM and MAOM is useful in understanding Hg sequestration in organic soils.

Early efforts to separate Hg speciation mainly focused on the chemical separation methods, e.g., sequential extraction procedures.[39−41] Most of these separation methods have more recently been questioned since the particular phase is strongly dependent on the extractant and procedure used.[39,42,43] Compared to chemical separation processes, physical separation based on size and/or density has gained favor for soil organic matter.[18,44] We proposed that analyzing the difference between POM-Hg and MAOM-Hg would show the potential to understand Hg dynamics in soil due to the different chemical constituents and functional groups. In this work, we determined the Hg, C, and N contents and their isotopic signatures in POM and MAOM samples collected from a deglaciated forest chronosequence to attribute the Hg sources. We chose a deglaciated forest chronosequence (i.e., a forest succession after glacier recession) as an extension to our earlier work,[45−47] discuss implications of the framework of POM-Hg versus MAOM-Hg in understanding Hg cycling in forest ecosystems, and make recommendations on future research needs.

2. METHODOLOGY

2.1. Site Description and Sample Collection. The selected deglaciated forest chronosequence locates at Mt. Gongga (101°59′ E, 29°34′ N, Figure 1) in the southeastern Tibetan Plateau at an elevation of 2950−3000 m above sea level. The glacier retreated area has a complete primary forest chronosequence over ∼2 km.[45−47] The vegetation in the deglaciated forest chronosequence varies from the pioneer species of deciduous broadleaf species including big leaf poplars (*Populus purdomii* Rehd.), common sea buckthorns

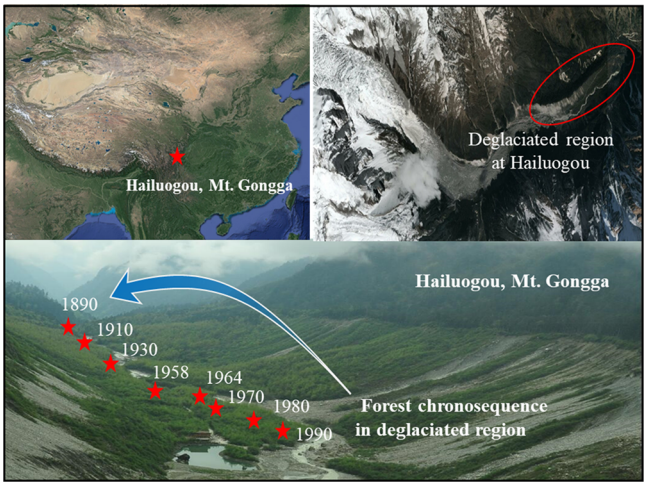

Figure 1. Sampling sites in a forest chronosequence at the deglaciated terrain of Hailuogou, Mt. Gongga in the Southeast Tibetan Plateau, China. The satellite image is from National Earth System Science Data Center, National Science & Technology Infrastructure of China (http://www.geodata.cn).

(*Hippophae rhamnoides* Linn.), and willows (*Salix magnifica* Hemsl.) at sites from 1990 to 1958 glacier retreat to the climax community of the Faber's firs (*Abies fabri (Mast.)* Craib) and dragon spruces (*Picea asperata* Mast.) at sites from 1930 to 1890.[47,48] The deglaciated forest chronosequence has an alpine monsoon climate with an annual mean temperature of 4 °C and precipitation of 1900 mm. The precipitation amount in the rainy season (May to October) accounts for ∼70% of the annual total precipitation.

Five broadleaf deciduous forest sites (i.e., 1990, 1980, 1970, 1964, and 1958) and three coniferous forest sites (i.e., 1930, 1910, and 1890) were selected for organic soil sampling in May 2022 (Figure 1). The detailed sampling protocols have been described in elsewhere.[45−47] Briefly, we set three 5 m × 5 m quadrats at each sampling site to collect organic soils. Within each quadrat, 5 replicate soil samples were collected (i.e., 4-corner and 1-center) and mixed to form one sample (mass of approximately 1−2 kg). The depth of organic soil in the deglaciated forest chronosequence varies with the glacier retreated time, e.g., 3 to 7 cm depth at sites 1990−1958 and ∼10 cm depth at sites 1930−1890. Our previous studies have shown that 0−6 cm depth of organic soil at sites 1930−1890 was formed by the decomposition of coniferous litters while >6 cm depth of organic soil was formed by long-term decomposition of deciduous litters.[47] To avoid the impacts caused by the different decomposing litters, we sampled the top 6 cm depth of organic soil at sites of 1930−1890.

2.2. POM and MAOM Fractionation. Soil organic matter components are operationally defined by size and density.[17−21] POM is defined as particulate organic matter with a size ranging from 53 to 2000 μm and a density less than 1.8 g cm^{-3}. Dissolved organic matter (DOM) is defined as water-soluble fraction that can pass through 0.45 μm filters. MAOM has multiple forms, including the small POM-like structures encapsulated by minerals, organic−mineral clusters, and primary organic−mineral complexes. We followed the separating protocol described elsewhere.[20,49] Briefly, 5 g of air-dried 2 mm-sieved soil was suspended in a solution of sodium polytungstate (1.8 g cm^{-3}) and allowed to settle overnight. We then collected the floating free-particulate

https://doi.org/10.1021/acs.est.3c03107
Environ. Sci. Technol. 2023, 57, 16512−16521

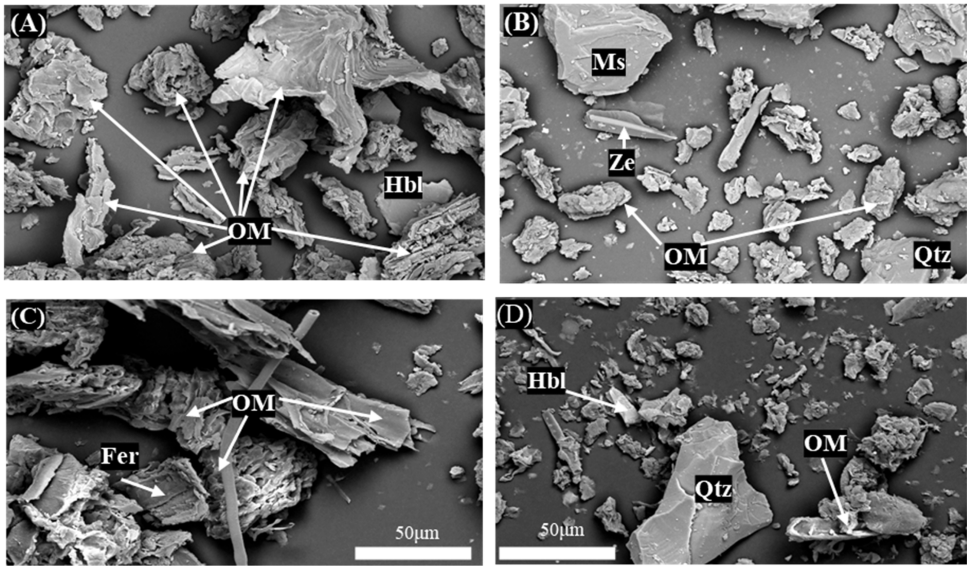

Figure 2. Scanning electron microscopy images of POM and MAOM. (A) POM at 1990 site, (B) MAOM at 1990 site, (C) POM at 1890 site, (D) MAOM at 1890 site. OM in (A)−(D) refers to organic matter, Hbl refers to Fer refers to fersmite, Ms refers to muscovite, Ze refers to zeolite, and Qtz refers to quartz. The SEM images at other sites are shown in Figures S2−S9.

organic matter. The remaining soil (>1.8 g cm^{-3}) was shaken at 180 r min^{-1} for 24 h to break up aggregates. After dispersion, soil samples were rinsed onto a 53 μm sieve. POM was collected as the fraction that remained on the sieve (>53 μm), and MAOM was collected as the insoluble fraction that passed through it (<53 μm). Then, we used a 0.45-μm membrane to separate the DOM from the MAOM fraction. The POM and MAOM were then oven-dried at 40 °C, weighed, and further analyzed. The recovery of soil mass after fractionation was between 94 and 98% (96 ± 3%, n = 63) of the initial sample weight. For the DOM solution which was extracted from the rinsewater, the 1% ultrapure hydrochloric acid was added and then stored in the 4 °C fridge.

2.3. Chemical Analysis. Hg concentrations of POM, MAOM, and 2 mm sieved soil organic matter (defined as TOM herein) were measured via combustion analysis coupled to atomic absorption spectroscopy using a DMA-80. We determined the Hg concentrations of one certified soil reference material and one parallel sample in each of the nine samples. The recovery of certified soil reference material (GSS-5, Hg concentration: 290 ± 30 ng g^{-1}, n = 12) ranged from 95% to 105%. The bias of the replicated sample was less than 5%. The Hg concentrations in DOM samples were determined by using a Tekran 2500 as the Hg detector. Figure S1 and Table S1 in the Supporting Information (SI) show the Hg mass balance in the POM and MAOM separating experiments. The ratio of Hg mass in the sum of POM, MAOM and DOM to the Hg mass in TOM across all samples is 94.4 ± 6.0% (n = 63), suggesting little Hg loss during the separating processes. The C and N concentrations in POM, MAOM, and TOM were measured by an Elementar Vario Macro Cube analyzer. Similarly, IVA99994 as the C and N standard was measured in every of the nine samples, which yielded recoveries of 97−105% (C: 100 ± 3%, n = 30; N: 101 ± 3%, n = 30). We also used scanning electron microscopy (SEM) and inductively coupled plasma optical emission spectroscopy (ICP-OES) to determine the mineralogical and chemical compositions of POM and MAOM. More details can be found in the SI.

The determination of Hg isotopic compositions has been described in our earlier work.[50,51] The POM, MAOM, and TOM soil samples were processed by double-stage heating pyrolysis in a tube muffle furnace. The Hg vapor from the sample was then captured using 5 mL of 40% reverse aqua regia (HCl: HNO_3 = 1:3, v/v) trapping solution.[52] The Hg concentration enriched in the trapping solution was measured by a Tekran 2500 following the US-EPA method 1631. The preconcentration recovery was in the range of 93−104% (97 ± 5%, n = 63). Stable Hg isotopes were determined by a multicollector inductively coupled plasma mass spectrometer (MC-ICP-MS, Nu-Plasma II). The enriched trapping solution was diluted to 1 ng mL^{-1} (10% acidity) and was then reduced by 3% $SnCl_2$ (i.e., stannous chloride) into Hg^0 in a cold vapor phase separator. Tl standard (i.e., thallium; NIST SRM 997) was coupled into the plasma as aerosol particulate through a CETAC Ardius II desolvating nebulizer system. Following Bergquist and Blum,[53] the Hg MDF is reported as

$$\delta^{202}\mathrm{Hg}\ (‰) = 1000 \times [(^{202}\mathrm{Hg}/^{198}\mathrm{Hg}_{\mathrm{sample}}) / (^{202}\mathrm{Hg}/^{198}\mathrm{Hg}_{\mathrm{NIST\text{-}3133}}) - 1] \quad (1)$$

where $(^{202}\mathrm{Hg}/^{198}\mathrm{Hg}_{\mathrm{NIST\text{-}3133}})$ represents the isotopic ratio in the standard sample (NIST-3133). MIF is calculated as

$$\Delta^{199}\mathrm{Hg}\ (‰) = \delta^{199}\mathrm{Hg} - 0.2520 \times \delta^{202}\mathrm{Hg} \quad (2)$$

$$\Delta^{200}\mathrm{Hg}\ (‰) = \delta^{200}\mathrm{Hg} - 0.5024 \times \delta \times \delta^{202}\mathrm{Hg} \quad (3)$$

$$\Delta^{201}\mathrm{Hg}\ (‰) = \delta^{201}\mathrm{Hg} - 0.7520 \times \delta^{202}\mathrm{Hg} \quad (4)$$

To evaluate whether isotopic composition bias occurs during preconcentration, we determined the Hg isotopic compositions of a certified soil reference material GSS-4. Results of GSS-4 were δ^{202}Hg = −1.83 ± 0.36‰, Δ^{199}Hg = −0.42 ± 0.06‰, Δ^{201}Hg = −0.41 ± 0.05‰, and Δ^{200}Hg = −0.02 ± 0.07‰ (mean ±2σ, n = 8). The NIST-8610 standard solution was measured every 10−15 samples as a secondary standard with results as δ^{202}Hg = −0.53 ± 0.09‰, Δ^{199}Hg = −0.01 ± 0.08‰, Δ^{201}Hg = −0.04 ± 0.05‰, and Δ^{200}Hg = −0.03 ±

https://doi.org/10.1021/acs.est.3c03107
Environ. Sci. Technol. 2023, 57, 16512−16521

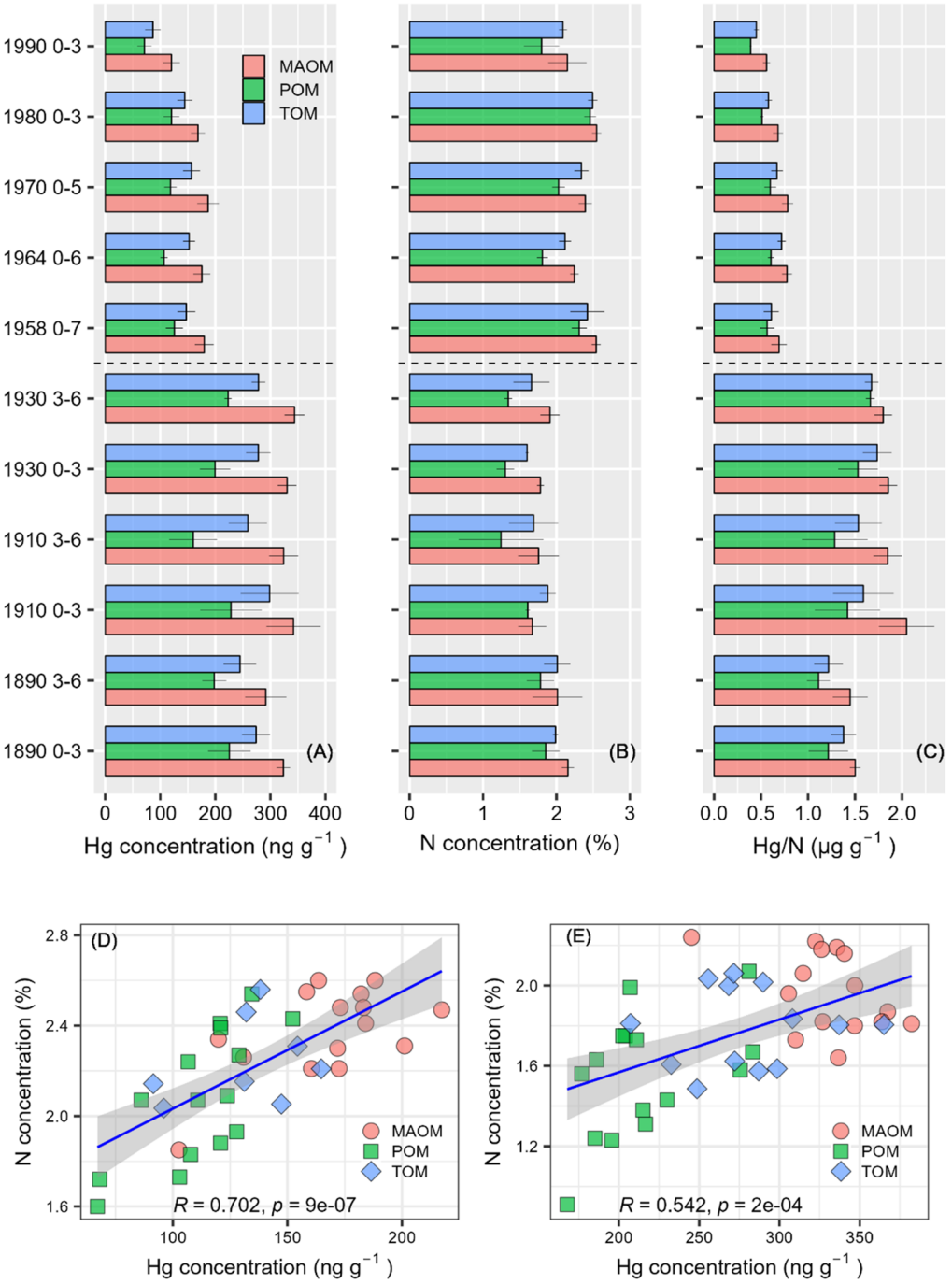

Figure 3. Mercury and nitrogen in soil MAOM (mineral associated organic matter with size <53 μm), POM (particulate organic matter with the size between 2000 and 53 μm), and TOM (total organic matter with size <2000 μm). (A) Hg concentration, (B) N concentration, (C) Hg/N ratio, (D) correlation between mercury and nitrogen at 1958−1990 broadleaf deciduous sites, and (E) correlation between mercury and nitrogen at 1930−1890 coniferous sites. The numbers after site names in (A)−(C) indicate the sampling depths of soil layers. The error bar in (A)−(C) stands for 1 standard error.

0.05‰ (mean $\pm 2\sigma$, n = 10). These measured values were consistent with the reported results, indicating negligible isotopic bias.[54,55]

The δ^{15}N ratios in POM, MAOM, and TOM soil samples were analyzed using a Thermo-Fisher MAT 253.[56] δ^{15}N and were calculated as follows:

$$\delta^{15}\mathrm{N}\ (‰) = 1000 \times [(^{15}\mathrm{N}/^{14}\mathrm{N}_{\mathrm{sample}})/(^{15}\mathrm{N}/^{14}\mathrm{N}_{\mathrm{air}}) - 1] \quad (5)$$

Standard samples of IAEA-NO_3 (i.e., potassium nitrate, KNO_3) were measured in each of the nine samples. Measured δ^{15}N for IAEA-NO_3 was 4.7 ± 0.4‰ (n = 42, recommended value = 4.7 ± 0.4‰).

2.4. Data Analysis. IBM SPSS Statistics v26.0 was utilized for statistical analysis at the 95% confidence level. We used One-Way ANOVA to determine significant differences of measured values at each forest site when data were normally distributed. Otherwise, the Kruskal−Wallis test was applied. We also used the Paired-t test to check the significance of Hg

https://doi.org/10.1021/acs.est.3c03107
Environ. Sci. Technol. 2023, 57, 16512−16521

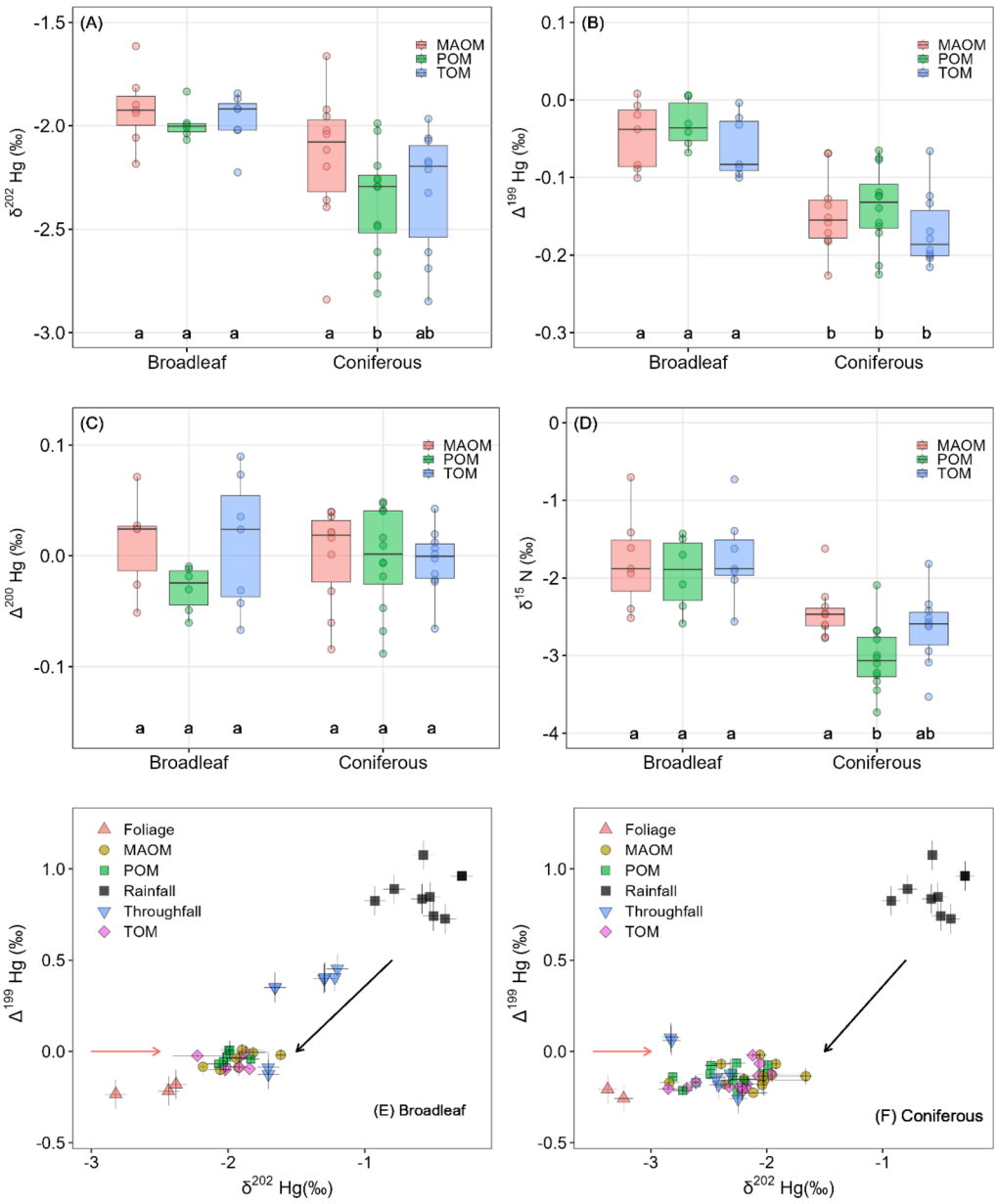

Figure 4. Mercury and nitrogen isotopic compositions in MAOM, POM, and TOM between 1958 and 1990 broadleaf deciduous sites and between 1930 and 1890 coniferous sites. (A) δ^{202}Hg, (B) Δ^{199}Hg, (C) Δ^{200}Hg, (D) δ^{15}N, (E) δ^{202}Hg versus Δ^{199}Hg at the 1958−1990 broadleaf deciduous sites, and (F) δ^{202}Hg versus Δ^{199}Hg at the 1930−1890 coniferous sites. The lowercase letters in (A)−(D) indicate the statistical difference at the 95% confidence level. Boxplot elements in (A)−(D) show the median (midline), the interquartile range of 25% and 75% percentile (box boundaries), and data points within the 1.5 × quartile range (whiskers). The error bars in (E) and (F) represent the 2 standard deviations. The black arrow in parts E and (F) represents the mixing of rainfall Hg, and the pink arrow represents the mixing of vegetation uptake Hg. The Hg isotopic signatures of rainfall, throughfall, and foliage are from our earlier studies.[47,48]

concentrations between POM and MAOM. Pearson correlation analysis was applied to evaluate the relation among variables.

3. RESULTS

3.1. Characteristics of OM and Measured Concentrations. Figures 2 and S2−S9 show scanning electron microscope (SEM) images of POM and MAOM across the deglaciated forest chronosequence. The SEM images displayed the distinct plant structures in POM samples and clustered organo-mineral structures in MAOM samples. POM is mainly composed of lightweight fragments that are relatively undecomposed. POM also contains small-sized minerals, mixed into lightweight fragments during the separation processes. For MAOM, mineral associations (e.g., fersmite, hornblende, quartz, clay, etc.) include chemical bonds between soil organic matter and mineral surface functional groups and the fraction trapped inside micropores or aggregates. Figure S10 shows significantly higher concentrations of Fe, Mn and Ti in MAOM samples compared to POM samples.

Figure 3 and Tables S2 and S3 show the results of Hg, C, and N concentrations and their stoichiometry in soil organic matter components. The Hg concentration in DOM ranged from 4.5 to 44.1 ng L^{-1}, with an average of 15.0 ± 7.7 ng L^{-1} (n = 33). Hg fraction in DOM is negligible (only 0.6% to 2.2% of total Hg mass) compared to those in POM and MAOM. In

https://doi.org/10.1021/acs.est.3c03107
Environ. Sci. Technol. 2023, 57, 16512−16521

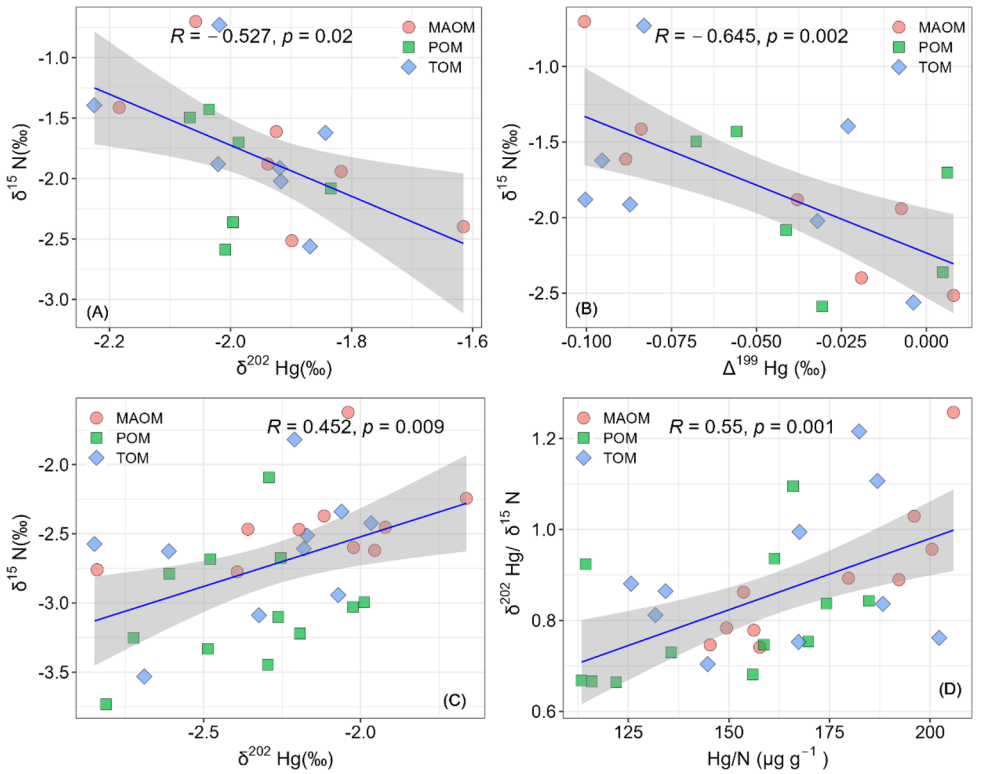

Figure 5. Correlations between mercury and nitrogen isotopic signatures in MAOM, POM, and TOM. (A) δ^{202}Hg versus δ^{15}N at 1958−1990 broadleaf deciduous sites, (B) Odd-MIF versus δ^{15}N at 1958−1990 broadleaf deciduous sites, (C) δ^{202}Hg versus δ^{15}N at 1930−1890 coniferous sites, and (D) δ^{202}Hg/ δ^{15}N versus Hg/N at 1930−1890 coniferous sites.

the broadleaf forests (including sites 1990, 1980,1970,1964, and 1958), site 1990 had the lowest Hg concentration in TOM (p < 0.05 by One-Way ANOVA test). The other four sites showed comparable concentrations (p > 0.05 by One-Way ANOVA test; Figure 3A). Hg concentrations (290−344 ng g^{-1}, 270 ± 50 ng g^{-1}) of TOM in the coniferous forests were comparable at the three sites (1930, 1910, and 1890; p > 0.05 by One-Way ANOVA test), but were 1−2 times higher than those (72 to 172 ng g^{-1}, 138 ± 29 ng g^{-1}) in the broadleaf forests. Intriguingly, the Hg concentration followed the trend of MAOM > TOM > POM across the whole forest chronosequence (MAOM: 249 ± 84 ng g^{-1}, n = 33; TOM: 206 ± 78 ng g^{-1}, n = 33; POM: 159 ± 64 ng g^{-1}, n = 33; p < 0.01 by the Paired-t test), with the Hg concentration in MAOM being 41−76% higher than that in POM of the broadleaf forests and 19−60% higher than that in POM of the coniferous forests. The Hg mass in MAOM accounted for 53%−79%, while that in POM accounted for 20%−46% of the total Hg mass in soil organic matter, depending on vegetation succession time (Figure S1).

Comparable C contents were observed among MAOM, POM, and TOM (Table S2 and Figure S11), while N contents showed a similar trend to that of Hg, i.e., MAOM > TOM > POM (Figure 3B), across the whole forest chronosequence (p < 0.01 by the Paired-t test). The N content in the soil samples of broadleaf forest was nearly 40% higher than that of the coniferous forest (p < 0.05 by One-Way ANOVA test). The Hg/N ratio in the broadleaf forest was 1−2 times smaller than that in the coniferous forest (Figure 3C). Among the soil organic matter components, the Hg/N and Hg/C ratios in MAOM are significantly higher than those in POM (p < 0.01 by the Paired-t test; Table S3). Additionally, the Hg concentration showed a significant correlation to N in both broadleaf and coniferous forests (Figure 3D,E).

3.2. Hg Isotopic Signatures. Figure 4 and Table S4 display the Hg isotopic signatures in the soil organic matter components. Comparable δ^{202}Hg values were observed between MAOM and POM components in the broadleaf forest chronosequence, with an average of −1.92 ± 0.14‰ (n = 8) in MAOM and −1.96 ± 0.14‰ (n = 8) in POM. In contrast, significantly higher δ^{202}Hg values were observed in MAOM than POM (−2.13 ± 0.30‰ versus −2.37 ± 0.26‰; p < 0.05 by the Paired-t test) in the coniferous forest chronosequence. δ^{15}N showed a asimilar trend to that of δ^{202}Hg. The Δ^{199}Hg of various organic fractions was similar for the same forest type, while the average Δ^{199}Hg of POM in the coniferous forest was significantly more negative than the value in the broadleaf forest (−0.14 ± 0.06‰ versus −0.05 ± 0.04‰; p < 0.05). The Δ^{199}Hg values of MAOM in the coniferous forest was also significantly more negative than the value in the broadleaf forest (−0.12 ± 0.06‰ versus −0.05 ± 0.04‰; p < 0.05). The Δ^{200}Hg signatures were close to 0 for all of the soil organic matter components across the forest chronosequence. Interestingly, δ^{15}N significantly anticorrelated with δ^{202}Hg and Δ^{199}Hg in the soil organic matter components of the broadleaf forest chronosequence (Figure 5A,B), while it significantly correlated with the δ^{202}Hg in the coniferous forest (Figure 5C). Besides, a significant correlation was also found between the ratio of δ^{202}Hg/δ^{15}N and the ratio of Hg/N in the coniferous forest (Figure 5D).

4. DISCUSSION

4.1. Hg Accumulation in Organic Matter Components. The Hg concentrations in soil organic matter

https://doi.org/10.1021/acs.est.3c03107
Environ. Sci. Technol. 2023, 57, 16512−16521

components of the coniferous forest are significantly higher than those in the broadleaf forest (Figure 3A). This is consistent with the earlier observations.[57−59] Higher Hg concentrations are often found in coniferous forest soil because of the elevated foliage Hg concentration (Figure S12) and deposition.[48] The 5−6 year lifespan of coniferous foliage increases atmospheric Hg^0 uptake compared to the several-month lifespan of broadleaf foliage.[22]

The significantly higher Hg concentrations in MAOM than in POM across the whole forest chronosequence suggest enhanced Hg accumulation in MAOM (Figure 3A). Although it has been suggested that fast C lost rate during the initial litter decomposition was the main cause for enriched Hg found in decomposed litter,[11,60] the C contents in POM and MAOM are comparable (Figure S11). This excludes the mass loss during initial litter decomposition as the only cause contributing to the elevated Hg in MAOM.

One possible reason for the enhanced Hg accumulation in MAOM is the longer exposure to Hg deposition considering its decades to centuries residence time, as compared to the <10-year residence time of POM.[17−21] Another possible reason is the selective Hg sorption to unique organic matter speciation of MAOM that are more conducive for Hg absorption and protective from litter decomposition via association with mineral surfaces.[18,19] Furthermore, the mineralogical and chemical compositions (Figures 2 and S2−S10) of POM and MAOM show clear differences in their physiochemical characteristics and persistence. Specifically, small size clay minerals and/or iron oxides which with large specific surface areas are enriched in MAOM, thus absorbing organic compounds complexed with Hg onto the surfaces.[17,61,62] Minerals can serve as catalysts for Hg^0 oxidation through direct electron transfer or by generating reactive oxygen species, which oxidize Hg^0 and stored the produced Hg^{2+}.[61,63]

4.2. Δ^{199}Hg Variations Determining Hg Sources in Soil Organic Matter Components. Atmospheric Hg depositions and geogenic Hg input (i.e., Hg releasing from rock weathering) are the main Hg sources in organic soils.[5,64] In this study, the geogenic Hg input is negligible due to the at least 1−2 orders of magnitude lower Hg concentration in the deep parent soil (2 ± 2 ng g^{-1}, $n = 15$) compared to the organic soil.[48,51] Therefore, the discussion is focused on organic soil.

The studied sites are far away from the influence of anthropogenic emissions, and thus, the Hg isotopic signatures in foliage, rainfall, and throughfall do not vary significantly over time. The similar Δ^{199}Hg signatures among soil organic matter components (Figure 4B) make Δ^{199}Hg a useful tracer for identifying the source contribution in organic soil. Our earlier work[48,51] showed that the Δ^{199}Hg values of throughfall Hg in the coniferous forest chronosequence are comparable to the Δ^{199}Hg values of atmospheric Hg^0, while those in the broadleaf forest chronosequence exhibit a range between signals of rainfall and atmospheric Hg^0. Throughfall Hg was derived from precipitation Hg and atmospheric Hg^0.[48,51] The throughfall in the coniferous forest chronosequence receives greater atmospheric Hg^0 because of the elevated Hg^0 uptake by foliage, moss, and lichen grown on the canopy and the subsequent detritus mixing into precipitation that contributes a large fraction of Hg in throughfall.[48,51]

The Δ^{199}Hg signatures of POM, MAOM, and TOM are similar to the Δ^{199}Hg of foliage, which represents the Δ^{199}Hg signature of atmospheric Hg^0. This suggests atmospheric Hg^0 deposition being the main Hg source in organic soil (Figure 4E,F), consistent with earlier observations in other forests.[31,65] The Δ^{199}Hg of soil organic matter components in the coniferous forest show insignificant difference ($p > 0.05$), while those in the broadleaf forest show a 0.05−0.1‰ positive shift from those of the atmospheric Hg^0 ($p < 0.05$). The more negative Δ^{199}Hg signatures in the coniferous forest point to a stronger influence of dry atmospheric Hg^0 deposition, consistent with the higher litterfall Hg concentration and throughfall deposition observed in our earlier work.[48]

4.3. δ^{202}Hg Variations Reflecting Hg Sequestration. The δ^{202}Hg signatures of soil organic matter components are significantly more positive than those in foliage (Figure 4E,F, both $p < 0.01$) of broadleaf and coniferous forests. This can be caused by the relatively positive δ^{202}Hg of throughfall Hg mixing into organic soil. The other cause is that the slow Hg loss via the microbial reduction can lead to heavier Hg isotopes being enriched into the organic soils.[60] We observed comparable Hg isotopic signatures between POM and MAOM in the broadleaf forest chronosequence but significantly more positive δ^{202}Hg in MAOM than POM in the coniferous forest chronosequence (Figure 4A,B, both $p < 0.01$). The difference can be explained by the Hg accumulation and sequestration processes during vegetation succession in the deglaciated forest chronosequence, illustrated as follows.

First, the initial Hg-DOM complexes stored in organic soil undergo negligible Hg isotopic fractionation,[66,67] and the separation of organic matter into POM and MAOM would not lead to a distinct MDF shift (Figure S13). In the events of precipitation, heavier Hg isotopes tend to be enriched in the dissolved phase in the form of Hg^{2+}.[68,69] The comparable Hg isotopic signatures between POM and MAOM in the broadleaf forest indicate that there are other processes involved in the postdeposition process other than Hg washout. The mineral−organic complexes contribute to the difference of δ^{202}Hg between MAOM and POM. It is known that soil minerals can influence organic contents and compositions in soil because of not-yet fully understood interfacial interactions and chemistry.[61,70] Similar to C, the Hg absorption and redox at the mineral-organic matter interface could induce δ^{202}Hg shifts different from plant-derived δ^{202}Hg in POM. Specifically, coniferous forests produce acidic soils that facilitate higher humic acid-rich DOM production compared to deciduous forests,[71,72] which further enhances dissolved Hg reactions at the mineral-organic interface.

Second, the chemical constituents and nutritional role of MAOM in the coniferous forest chronosequence may lead to a different Hg sequestration process. POM is readily more bioavailable, but usually contains larger and insoluble molecules and therefore requires depolymerization prior to assimilation.[17−20] In contrast, components in MAOM tend to be more nutrient dense (higher N as shown in Figure 3B). Once dissociated from the minerals, MAOM can be quickly assimilated or decomposed.[18,19] The chemistry and nutrient of the plant input control the quality of POM for microbiota uptake.[18,19] The litters of coniferous forests have low N contents (Figure S12) and high levels of recalcitrant and nonbiodegradable components.[73] Compared to POM, MAOM in the coniferous forest chronosequence is likely to be more useful to microbiota as a labile carbon and nutrient source. Thus, microbial reduction during MAOM mineralization could enrich heavier Hg isotopes accumulated into MAOM. Another possible cause is the absorption of residual Hg with positive

https://doi.org/10.1021/acs.est.3c03107
Environ. Sci. Technol. 2023, 57, 16512−16521

δ^{202}Hg by MAOM from previous Hg biogeochemical processes in soil solution, such as the residual Hg with enriched ^{202}Hg during DOM mediated Hg reduction.[24,25]

Correlation analysis between N and Hg isotopic signatures provides additional insights into Hg accumulation and sequestration processes. N can form the metal-binding functional groups (e.g., N/O) and control the microbial community diversity and chemodiversity of soil organic matter.[5,11,45,46] The δ^{15}N increases with the decreasing C/N ratio (Figure S14). This suggests an increase of humified carbon and an associated increase in aliphaticity.[70] Throughfall in the broadleaf forest chronosequence is associated with more positive δ^{202}Hg and Δ^{199}Hg signals, but more negative δ^{15}N values in contrast to the signals in foliage litters (Table S4). The negative correlations between δ^{202}Hg and δ^{15}N, and between Δ^{199}Hg and δ^{15}N (Figure 5A,B) reflect the input mixing of throughfall and litterfall. The increase of litterfall and throughfall input during vegetation succession increases nutrient input and chemical stability of soil organic matter, and microbial community diversity, as well as promotes Hg and N fixation in the organic soil.[73] Therefore, variation of δ^{202}Hg in soil organic matter depends on the δ^{202}Hg shifts in each source endmember. Figure 5C depicts the positive correlation between δ^{202}Hg and δ^{15}N in the coniferous forest chronosequence. Figure 5D shows that δ^{202}Hg/δ^{15}N increases with increasing Hg/N ratio. These correlations suggest that changes in Hg and N isotopic signatures are synchronous to Hg and N contents in organic soil. These correlations reflect the effect of microbial reduction and mineralization that facilitates the accumulation of heavier Hg and N isotopes in soil organic matter components.[5,11,45,46]

Finally, an δ^{202}Hg mass balance between litterfall and throughfall was performed to assess their respective contribution to the change of soil δ^{202}Hg. The results (Figure S15) showed that the predicted δ^{202}Hg (based on the mass balance of deposition flux) is more negative than the observed δ^{202}Hg ($p < 0.05$ by Paired-t test) in the surface soil at sites of 1880−1960 (the coniferous forest chronosequence), but consistent to the δ^{202}Hg values at sites of 1965−1990 (the broadleaf forest chronosequence). These further validated our hypothesis that the change of δ^{202}Hg in soil organic matter components is controlled by the input mixing of throughfall and litterfall in the broadleaf forest and that microbial reduction and mineralization enrich heavier Hg isotopes in the coniferous forest.

5. IMPLICATIONS

In this study, we show that elevated accumulation of atmospheric Hg^0 and subsequent microbial reduction enrich heavier Hg isotopes in MAOM compared to POM due to the specific MAOM chemical constituents and nutritional role. The individual isotopic evidence shown in the POM and MAOM fractions improves our understanding of Hg cycling in organic soils. Our results also show the strong relations between Hg and N in both concentration and isotopic signatures in the soil organic matter components. Currently, there are few data of Hg speciation in background organic soil, due to the challenge of Hg speciation measurement at low Hg concentration even by advanced analytical techniques such as X-ray absorption near edge structure (XANES) spectroscopy.[15,74] In this study, we demonstrated an analytical framework of POM-Hg and MAOM-Hg for understanding and predicting Hg biogeochemical processes in organic soil. This methodology represents a practical approach for gaining process insights into Hg cycling in forest ecosystems. Specifically, the broad scale measurements of POM and MAOM have been performed in organic matter community, and the framework of POM versus MAOM is already incorporated into newer generation soil organic matter models.[18,44] Using the presented data, we conclude that Hg source mixing controls Hg isotopic variation in the younger broadleaf forest, while postdeposition processes are the primary driver in the older coniferous forest.

■ ASSOCIATED CONTENT

Supporting Information

The Supporting Information is available free of charge at https://pubs.acs.org/doi/10.1021/acs.est.3c03107.

Additional data for Hg signatures in Tables S1−S4; additional figures as mentioned in the text (Figures S1−S15) (PDF)

■ AUTHOR INFORMATION

Corresponding Author

Xun Wang − *State Key Laboratory of Environmental Geochemistry, Institute of Geochemistry, Chinese Academy of Sciences, Guiyang 550081, China;* orcid.org/0000-0002-7407-8965; Email: wangxun@mail.gyig.ac.cn

Authors

Fei Wu − *State Key Laboratory of Environmental Geochemistry, Institute of Geochemistry, Chinese Academy of Sciences, Guiyang 550081, China; University of Chinese Academy of Sciences, Beijing 100049, China*

Luhan Yang − *College of Resources and Environment, Southwest University, Chongqing 400715, China*

Wei Yuan − *State Key Laboratory of Environmental Geochemistry, Institute of Geochemistry, Chinese Academy of Sciences, Guiyang 550081, China;* orcid.org/0000-0003-3329-2081

Che-Jen Lin − *Center for Advances in Water and Air Quality, Lamar University, Beaumont, Texas 77710, United States*

Xinbin Feng − *State Key Laboratory of Environmental Geochemistry, Institute of Geochemistry, Chinese Academy of Sciences, Guiyang 550081, China;* orcid.org/0000-0002-7462-8998

Complete contact information is available at: https://pubs.acs.org/10.1021/acs.est.3c03107

Notes

The authors declare no competing financial interest.

■ ACKNOWLEDGMENTS

This work was funded by National Natural Science Foundation of China (41977272 and 42122053).

■ REFERENCES

(1) Selin, H.; Selin, N. E. From Stockholm to Minamata and beyond: Governing mercury pollution for a more sustainable future. *One Earth* **2022**, *5* (10), 1109−1125.

(2) Wang, X.; Yuan, W.; Lin, C.-J.; Wang, D.; Luo, J.; Xia, J.; Zhang, W.; Wang, F.; Feng, X. Root uptake dominates mercury accumulation in permafrost plants of Qinghai-Tibet Plateau. *Communications Earth & Environment* **2022**, *3*, 287 DOI: 10.1038/s43247-022-00619-y.

(3) Wu, Q.; Zhang, Y.; Li, P.; Fu, X.; Zhang, Q.; Wang, X.; Chen, L.; Wang, S.; Wang, F.; Feng, X. Ecosystem Mercury Recovery and Health Benefit Under the Minamata Convention in a Changing

Climate. *Reviews of Environmental Contamination and Toxicology* **2022**, DOI: 10.1007/s44169-022-00016-8.
(4) Wang, X.; Bao, Z.; Lin, C.-J.; Yuan, W.; Feng, X. Assessment of Global Mercury Deposition through Litterfall. *Environ. Sci. Technol.* **2016**, *50* (16), 8548−8557.
(5) Wang, X.; Yuan, W.; Lin, C.-J.; Feng, X. Mercury cycling and isotopic fractionation in global forests. *Crit Rev. Env Sci. Tec* **2022**, *52* (21), 3763−3786.
(6) Wang, X.; Yuan, W.; Lin, C. J.; Zhang, L.; Zhang, H.; Feng, X. Climate and Vegetation As Primary Drivers for Global Mercury Storage in Surface Soil. *Environ. Sci. Technol.* **2019**, *53* (18), 10665−10675.
(7) Obrist, D.; Johnson, D. W.; Lindberg, S. E.; Luo, Y.; Hararuk, O.; Bracho, R.; Battles, J. J.; Dail, D. B.; Edmonds, R. L.; Monson, R. K.; Ollinger, S. V.; Pallardy, S. G.; Pregitzer, K. S.; Todd, D. E. Mercury Distribution Across 14 US Forests. Part I: Spatial Patterns of Concentrations in Biomass, Litter, and Soils. *Environ. Sci. Technol.* **2011**, *45* (9), 3974−3981.
(8) Obrist, D.; Kirk, J. L.; Zhang, L.; Sunderland, E. M.; Jiskra, M.; Selin, N. E. A review of global environmental mercury processes in response to human and natural perturbations: Changes of emissions, climate, and land use. *Ambio* **2018**, *47* (2), 116−140.
(9) Demers, J. D.; Yavitt, J. B.; Driscoll, C. T.; Montesdeoca, M. R. Legacy mercury and stoichiometry with C, N, and S in soil, pore water, and stream water across the upland-wetland interface: The influence of hydrogeologic setting. *J. Geophys Res-Biogeo* **2013**, *118* (2), 825−841.
(10) Grigal, D. F. Mercury sequestration in forests and peatlands: A review. *J. Environ. Qual* **2003**, *32* (2), 393−405.
(11) Wang, X.; Lin, C.-J.; Lu, Z.; Zhang, H.; Zhang, Y.; Feng, X. Enhanced accumulation and storage of mercury on subtropical evergreen forest floor: Implications on mercury budget in global forest ecosystems. *J. Geophys Res-Biogeo* **2016**, *121* (8), 2096−2109.
(12) Gu, B.; Bian, Y.; Miller, C. L.; Dong, W.; Jiang, X.; Liang, L. Mercury reduction and complexation by natural organic matter in anoxic environments. *Proc. Natl. Acad. Sci. U. S. A.* **2011**, *108* (4), 1479−1483.
(13) Si, L.; Ariya, P. A. Reduction of oxidized mercury species by dicarboxylic acids (C(2)-C(4)): Kinetic and product studies. *Environ. Sci. Technol.* **2008**, *42* (14), 5150−5155.
(14) Zheng, W.; Liang, L.; Gu, B. Mercury Reduction and Oxidation by Reduced Natural Organic Matter in Anoxic Environments. *Environ. Sci. Technol.* **2012**, *46* (1), 292−299.
(15) Manceau, A.; Lemouchi, C.; Enescu, M.; Gaillot, A. C.; Lanson, M.; Magnin, V.; Glatzel, P.; Poulin, B. A.; Ryan, J. N.; Aiken, G. R.; Gautier-Luneau, I.; Nagy, K. L. Formation of Mercury Sulfide from Hg(II)-Thiolate Complexes in Natural Organic Matter. *Environ. Sci. Technol.* **2015**, *49* (16), 9787−9796.
(16) Lei, P.; Zhang, J.; Zhu, J.; Tan, Q.; Kwong, R. W. M.; Pan, K.; Jiang, T.; Naderi, M.; Zhong, H. Algal Organic Matter Drives Methanogen-Mediated Methylmercury Production in Water from Eutrophic Shallow Lakes. *Environ. Sci. Technol.* **2021**, *55*, 10811.
(17) Weng, Z.; Lehmann, J.; Van Zwieten, L.; Joseph, S.; Archanjo, B. S.; Cowie, B.; Thomsen, L.; Tobin, M. J.; Vongsvivut, J.; Klein, A.; Doolette, C. L.; Hou, H. E.; Mueller, C. W.; Lombi, E.; Kopittke, P. M. Probing the nature of soil organic matter. *Crit Rev. Env Sci. Tec* **2022**, *52* (22), 4072−4093.
(18) Lavallee, J. M.; Soong, J. L.; Cotrufo, M. F. Conceptualizing soil organic matter into particulate and mineral-associated forms to address global change in the 21st century. *Glob Chang Biol.* **2020**, *26* (1), 261−273.
(19) Witzgall, K.; Vidal, A.; Schubert, D. I.; Hoschen, C.; Schweizer, S. A.; Buegger, F.; Pouteau, V.; Chenu, C.; Mueller, C. W. Particulate organic matter as a functional soil component for persistent soil organic carbon. *Nat. Commun.* **2021**, *12* (1), 4115.
(20) Lugato, E.; Lavallee, J. M.; Haddix, M. L.; Panagos, P.; Cotrufo, M. F. Different climate sensitivity of particulate and mineral-associated soil organic matter. *Nature Geoscience* **2021**, *14* (5), 295−300.
(21) Steffens, M.; Zeh, L.; Rogge, D. M.; Buddenbaum, H. Quantitative mapping and spectroscopic characterization of particulate organic matter fractions in soil profiles with imaging VisNIR spectroscopy. *Sci. Rep* **2021**, *11* (1), 16725.
(22) Zeng, S.; Wang, X.; Yuan, W.; Luo, J.; Wang, D. Mercury accumulation and dynamics in montane forests along an elevation gradient in Southwest China. *J. Environ. Sci. (China)* **2022**, *119*, 1−10.
(23) Gong, P.; Wang, X.-p.; Xue, Y.-g.; Xu, B.-q.; Yao, T.-d. Mercury distribution in the foliage and soil profiles of the Tibetan forest: Processes and implications for regional cycling. *Environ. Pollut.* **2014**, *188*, 94−101.
(24) Zheng, W.; Hintelmann, H. Isotope Fractionation of Mercury during Its Photochemical Reduction by Low-Molecular-Weight Organic Compounds. *J. Phys. Chem. A* **2010**, *114* (12), 4246−4253.
(25) Zheng, W.; Hintelmann, H. Nuclear Field Shift Effect in Isotope Fractionation of Mercury during Abiotic Reduction in the Absence of Light. *J. Phys. Chem. A* **2010**, *114* (12), 4238−4245.
(26) Kritee, K.; Blum, J. D.; Barkay, T. Mercury Stable Isotope Fractionation during Reduction of Hg(II) by Different Microbial Pathways. *Environ. Sci. Technol.* **2008**, *42* (24), 9171−9177.
(27) Kritee, K.; Blum, J. D.; Johnson, M. W.; Bergquist, B. A.; Barkay, T. Mercury stable isotope fractionation during reduction of Hg(II) to Hg(0) by mercury resistant microorganisms. *Environ. Sci. Technol.* **2007**, *41* (6), 1889−1895.
(28) Jiskra, M.; Wiederhold, J. G.; Skyllberg, U.; Kronberg, R. M.; Hajdas, I.; Kretzschmar, R. Mercury deposition and re-emission pathways in boreal forest soils investigated with Hg isotope signatures. *Environ. Sci. Technol.* **2015**, *49* (12), 7188−7196.
(29) Motta, L. C.; Kritee, K.; Blum, J. D.; Tsz-Ki Tsui, M.; Reinfelder, J. R. Mercury Isotope Fractionation during the Photochemical Reduction of Hg(II) Coordinated with Organic Ligands. *J. Phys. Chem. A* **2020**, *124* (14), 2842−2853.
(30) Chen, J.; Hintelmann, H.; Feng, X.; Dimock, B. Unusual fractionation of both odd and even mercury isotopes in precipitation from Peterborough, ON, Canada. *Geochim Cosmochim Ac* **2012**, *90*, 33−46.
(31) Demers, J. D.; Blum, J. D.; Zak, D. R. Mercury isotopes in a forested ecosystem: Implications for air-surface exchange dynamics and the global mercury cycle. *Global Biogeochemical Cycles* **2013**, *27* (1), 222−238.
(32) Li, K.; Lin, C. J.; Yuan, W.; Sun, G. Y.; Fu, X. W.; Feng, X. B. An improved method for recovering and preconcentrating mercury in natural water samples for stable isotope analysis. *Journal of Analytical Atomic Spectrometry* **2019**, *34* (11), 2303−2313.
(33) Gratz, L. E.; Keeler, G. J.; Blum, J. D.; Sherman, L. S. Isotopic composition and fractionation of mercury in Great Lakes precipitation and ambient air. *Environ. Sci. Technol.* **2010**, *44* (20), 7764−7770.
(34) Yuan, W.; Wang, X.; Lin, C.-J.; Wu, C.; Zhang, L.; Wang, B.; Sommar, J.; Lu, Z.; Feng, X. Stable Mercury Isotope Transition during Postdepositional Decomposition of Biomass in a Forest Ecosystem over Five Centuries. *Environ. Sci. Technol.* **2020**, *54* (14), 8739−8749.
(35) Xia, S.; Yuan, W.; Lin, L.; Yang, X.; Feng, X.; Li, X.; Liu, X.; Chen, P.; Zeng, S.; Wang, D.; Su, Q.; Wang, X. Latitudinal gradient for mercury accumulation and isotopic evidence for post-depositional processes among three tropical forests in Southwest China. *J. Hazard Mater.* **2022**, *429*, 128295.
(36) Guedron, S.; Arnouroux, D.; Tessier, E.; Grirnaldi, C.; Barre, J.; Berail, S.; Perrot, V.; Grimaldi, M. Mercury Isotopic Fractionation during Pedogenesis in a Tropical Forest Soil Catena (French Guiana): Deciphering the Impact of Historical Gold Mining. *Environ. Sci. Technol.* **2018**, *52* (20), 11573−11582.
(37) Sun, R.; Jiskra, M.; Amos, H. M.; Zhang, Y.; Sunderland, E. M.; Sonke, J. E. Modelling the mercury stable isotope distribution of Earth surface reservoirs: Implications for global Hg cycling. *Geochim. Cosmochim. Acta* **2019**, *246*, 156−173.
(38) Blum, J. D.; Sherman, L. S.; Johnson, M. W. Mercury Isotopes in Earth and Environmental Sciences. *Annual Review of Earth and Planetary Sciences* **2014**, *42*, 249−269.

(39) Sladek, C.; Gustin, M. S. Evaluation of sequential and selective extraction methods for determination of mercury speciation and mobility in mine waste. *Appl. Geochem.* **2003**, *18* (4), 567−576.
(40) Fernandez-Martinez, R.; Loredo, J.; Ordonez, A.; Rucandio, M. I. Physicochemical characterization and mercury speciation of particle-size soil fractions from an abandoned mining area in Mieres, Asturias (Spain). *Environ. Pollut.* **2006**, *142* (2), 217−226.
(41) Tessier, A.; Campbell, P. G. C.; Bisson, M. Sequential Extraction Procedure for the Speciation of Particulate Trace-Metals. *Anal. Chem.* **1979**, *51* (7), 844−851.
(42) Bacon, J. R.; Davidson, C. M. Is there a future for sequential chemical extraction? *Analyst* **2008**, *133* (1), 25−46.
(43) Dong, H.; Feng, L.; Qin, Y.; Luo, M. Comparison of different sequential extraction procedures for mercury fractionation in polluted soils. *Environ. Sci. Pollut Res. Int.* **2019**, *26* (10), 9955−9965.
(44) Heckman, K. A.; Possinger, A. R.; Badgley, B. D.; Bowman, M. M.; Gallo, A. C.; Hatten, J. A.; Nave, L. E.; SanClements, M. D.; Swanston, C. W.; Weiglein, T. L.; Wieder, W. R.; Strahm, B. D. Moisture-driven divergence in mineral-associated soil carbon persistence. *Proc. Natl. Acad. Sci. U. S. A.* **2023**, *120* (7), e2210044120.
(45) Wang, X.; Luo, J.; Lin, C.-J.; Wang, D.; Yuan, W. Elevated cadmium pollution since 1890s recorded by forest chronosequence in deglaciated region of Gongga, China. *Environ. Pollut.* **2020**, *260*, 114082.
(46) Wang, X.; Yuan, W.; Feng, X.; Wang, D.; Luo, J. Moss facilitating mercury, lead and cadmium enhanced accumulation in organic soils over glacial erratic at Mt. Gongga, China. *Environ. Pollut.* **2019**, *254*, 112974.
(47) Wang, X.; Luo, J.; Yuan, W.; Lin, C. J.; Wang, F.; Liu, C.; Wang, G.; Feng, X. Global warming accelerates uptake of atmospheric mercury in regions experiencing glacier retreat. *Proc. Natl. Acad. Sci. U. S. A.* **2020**, *117* (4), 2049−2055.
(48) Wang, X.; Yuan, W.; Lin, C. J.; Luo, J.; Wang, F.; Feng, X.; Fu, X.; Liu, C. Underestimated Sink of Atmospheric Mercury in a Deglaciated Forest Chronosequence. *Environ. Sci. Technol.* **2020**, *54* (13), 8083−8093.
(49) Martens, J.; Mueller, C. W.; Joshi, P.; Rosinger, C.; Maisch, M.; Kappler, A.; Bonkowski, M.; Schwamborn, G.; Schirrmeister, L.; Rethemeyer, J. Stabilization of mineral-associated organic carbon in Pleistocene permafrost. *Nat. Commun.* **2023**, *14* (1), 2120.
(50) Wang, X.; Luo, J.; Yin, R.; Yuan, W.; Lin, C. J.; Sommar, J.; Feng, X.; Wang, H.; Lin, C. Using Mercury Isotopes To Understand Mercury Accumulation in the Montane Forest Floor of the Eastern Tibetan Plateau. *Environ. Sci. Technol.* **2017**, *51* (2), 801−809.
(51) Wang, X.; Luo, J.; Yuan, W.; Lin, C.-J.; Wang, F.; Liu, C.; Wang, G.; Feng, X. Global warming accelerates uptake of atmospheric mercury in regions experiencing glacier retreat. *Proc. Natl. Acad. Sci. U. S. A.* **2020**, *117* (4), 2049−2055.
(52) Sun, R. Y.; Enrico, M.; Heimburger, L. E.; Scott, C.; Sonke, J. E. A double-stage tube furnace-acid-trapping protocol for the pre-concentration of mercury from solid samples for isotopic analysis. *Anal Bioanal Chem.* **2013**, *405* (21), 6771−6781.
(53) Bergquist, B. A.; Blum, J. D. Mass-Dependent and -Independent Fractionation of Hg Isotopes by Photoreduction in Aquatic Systems. *Science* **2007**, *318* (5849), 417−420.
(54) Estrade, N.; Carignan, J.; Sonke, J. E.; Donard, O. F. X. Measuring Hg Isotopes in Bio-Geo-Environmental Reference Materials. *Geostand Geoanal Res.* **2010**, *34* (1), 79−93.
(55) Blum, J. D.; Bergquist, B. A. Reporting of variations in the natural isotopic composition of mercury. *Anal Bioanal Chem.* **2007**, *388* (2), 353−359.
(56) Radke, J.; Deerberg, M.; Hilkert, A.; Schlüter, H. J.; Schwieters, J. High Resolution Double-Focusing Isotope Ratio Mass Spectrometry. *Egu General Assembly* **2012**, *14* (23), 12549.
(57) Mendez-Lopez, M.; Gomez-Armesto, A.; Alonso-Vega, F.; Pontevedra-Pombal, X.; Fonseca, F.; de Figueiredo, T.; Arias-Estevez, M.; Novoa-Munoz, J. C. The role of afforestation species as a driver of Hg accumulation in organic horizons of forest soils from a Mediterranean mountain area in SW Europe. *Sci. Total Environ.* **2022**, *827*, 154345.
(58) Mendez-Lopez, M.; Parente-Sendin, A.; Calvo-Portela, N.; Gomez-Armesto, A.; Eimil-Fraga, C.; Alonso-Vega, F.; Arias-Estevez, M.; Novoa-Munoz, J. C. Mercury in a birch forest in SW Europe: Deposition flux by litterfall and pools in aboveground tree biomass and soils. *Sci. Total Environ.* **2023**, *856* (Pt 1), 158937.
(59) Obrist, D.; Johnson, D. W.; Edmonds, R. L. Effects of vegetation type on mercury concentrations and pools in two adjacent coniferous and deciduous forests. *J. Plant Nutr Soil Sc* **2012**, *175* (1), 68−77.
(60) Yuan, W.; Wang, X.; Lin, C. J.; Wu, C.; Zhang, L.; Wang, B.; Sommar, J.; Lu, Z.; Feng, X. Stable Mercury Isotope Transition during Postdepositional Decomposition of Biomass in a Forest Ecosystem over Five Centuries. *Environ. Sci. Technol.* **2020**, *54* (14), 8739−8749.
(61) Kleber, M.; Bourg, I. C.; Coward, E. K.; Hansel, C. M.; Myneni, S. C. B.; Nunan, N. Dynamic interactions at the mineral-organic matter interface. *Nature Reviews Earth & Environment* **2021**, *2*, 402.
(62) Quenea, K.; Lamy, I.; Winterton, P.; Bermond, A.; Dumat, C. Interactions between metals and soil organic matter in various particle size fractions of soil contaminated with waste water. *Geoderma* **2009**, *149* (3), 217−223.
(63) Jiskra, M.; Saile, D.; Wiederhold, J. G.; Bourdon, B.; Bjorn, E.; Kretzschmar, R. Kinetics of Hg(II) exchange between organic ligands, goethite, and natural organic matter studied with an enriched stable isotope approach. *Environ. Sci. Technol.* **2014**, *48* (22), 13207−13217.
(64) Lindberg, S.; Bullock, R.; Ebinghaus, R.; Engstrom, D.; Feng, X.; Fitzgerald, W.; Pirrone, N.; Prestbo, E.; Seigneur, C. Panel on Source Attribution of Atmospheric, M. A synthesis of progress and uncertainties in attributing the sources of mercury in deposition. *Ambio* **2007**, *36* (1), 19−32.
(65) Yuan, W.; Wang, X.; Lin, C. J.; Sommar, J. O.; Wang, B.; Lu, Z.; Feng, X. Quantification of Atmospheric Mercury Deposition to and Legacy Re-emission from a Subtropical Forest Floor by Mercury Isotopes. *Environ. Sci. Technol.* **2021**, *55* (18), 12352−12361.
(66) Jiskra, M.; Wiederhold, J. G.; Skyllberg, U.; Kronberg, R. M.; Kretzschmar, R. Source tracing of natural organic matter bound mercury in boreal forest runoff with mercury stable isotopes. *Environ. Sci. Process Impacts* **2017**, *19* (10), 1235−1248.
(67) Woerndle, G. E.; Tsz-Ki Tsui, M.; Sebestyen, S. D.; Blum, J. D.; Nie, X.; Kolka, R. K. New Insights on Ecosystem Mercury Cycling Revealed by Stable Isotopes of Mercury in Water Flowing from a Headwater Peatland Catchment. *Environ. Sci. Technol.* **2018**, *52* (4), 1854−1861.
(68) Jiskra, M.; Wiederhold, J. G.; Bourdon, B.; Kretzschmar, R. Solution speciation controls mercury isotope fractionation of Hg(II) sorption to goethite. *Environ. Sci. Technol.* **2012**, *46* (12), 6654−6662.
(69) Wiederhold, J. G.; Cramer, C. J.; Daniel, K.; Infante, I.; Bourdon, B.; Kretzschmar, R. Equilibrium mercury isotope fractionation between dissolved Hg(II) species and thiol-bound Hg. *Environ. Sci. Technol.* **2010**, *44* (11), 4191−4197.
(70) Kramer, M. G.; Lajtha, K.; Aufdenkampe, A. K. Depth trends of soil organic matter C:N and 15N natural abundance controlled by association with minerals. *Biogeochemistry* **2017**, *136* (3), 237−248.
(71) Rydberg, J.; Rosch, M.; Heinz, E.; Biester, H. Influence of catchment vegetation on mercury accumulation in lake sediments from a long-term perspective. *Sci. Total Environ.* **2015**, *538*, 896−904.
(72) Schütze, M.; Gatz, P.; Gilfedder, B. S.; Biester, H. Why productive lakes are larger mercury sedimentary sinks than oligotrophic brown water lakes. *Limnol Oceanogr* **2021**, *66* (4), 1316−1332.
(73) Yu, S.; Lv, J.; Jiang, L.; Geng, P.; Cao, D.; Wang, Y. Changes of Soil Dissolved Organic Matter and Its Relationship with Microbial Community along the Hailuogou Glacier Forefield Chronosequence. *Environ. Sci. Technol.* **2023**, *57*, 4027.
(74) Wang, J.; Man, Y.; Yin, R.; Feng, X. Isotopic and Spectroscopic Investigation of Mercury Accumulation in Houttuynia cordata Colonizing Historically Contaminated Soil. *Environ. Sci. Technol.* **2022**, *56* (12), 7997−8007.

https://doi.org/10.1021/acs.est.3c03107
Environ. Sci. Technol. 2023, 57, 16512−16521